Missouri University of Science and Technology
Scholars' Mine

Geosciences and Geological and Petroleum Engineering Faculty Research & Creative Works

Geosciences and Geological and Petroleum Engineering

01 Jan 2023

Sedimentological And Geochemical Characterization Of A Varved Sediment Record From The Northern Neotropics

Edward Duarte

Jonathan Obrist-Farner
Missouri University of Science and Technology, obristj@mst.edu

Susan R.H. Zimmerman

Erik T. Brown

et. al. For a complete list of authors, see https://scholarsmine.mst.edu/geosci_geo_peteng_facwork/2174

Follow this and additional works at: https://scholarsmine.mst.edu/geosci_geo_peteng_facwork

 Part of the Geological Engineering Commons, and the Petroleum Engineering Commons

Recommended Citation

E. Duarte et al., "Sedimentological And Geochemical Characterization Of A Varved Sediment Record From The Northern Neotropics," *Journal of Paleolimnology*, Springer, Jan 2023.
The definitive version is available at https://doi.org/10.1007/s10933-023-00292-x

This Article - Journal is brought to you for free and open access by Scholars' Mine. It has been accepted for inclusion in Geosciences and Geological and Petroleum Engineering Faculty Research & Creative Works by an authorized administrator of Scholars' Mine. This work is protected by U. S. Copyright Law. Unauthorized use including reproduction for redistribution requires the permission of the copyright holder. For more information, please contact scholarsmine@mst.edu.

J Paleolimnol
https://doi.org/10.1007/s10933-023-00292-x

ORIGINAL PAPER

Sedimentological and geochemical characterization of a varved sediment record from the northern Neotropics

Edward Duarte · Jonathan Obrist-Farner · Susan R. H. Zimmerman · Erik T. Brown · Robert Brown

Received: 19 August 2022 / Accepted: 12 June 2023
© The Author(s), under exclusive licence to Springer Nature B.V. 2023

Abstract Annually resolved sedimentological records (including annual varves) can be used to develop precise chronologies for key climatic and tectonic events. Varved records, however, are most common in high latitude lakes, resulting in a spatial bias with respect to annually resolved records in tropical regions. Here we report on the sedimentology of two sediment cores from Lake Izabal, eastern Guatemala, that contain a well-preserved thinly laminated section spanning ca. 2200 years of the mid-Holocene. We integrate radiocarbon age-depth modeling, sedimentological observations, laminae counting, μX-ray fluorescence scanning, and multivariate statistical analyses to constrain the nature and chronology of the laminations. Our sedimentological and geochemical results suggest that the alternating clastic (dark) and biogenic (light) laminae couplets were deposited annually. Dark laminae are characterized by an abundance of detrital grains, organic detritus, total organic carbon, and terrigenic elements, and most likely formed during times of increased discharge during the rainy season. In contrast, light laminae are characterized by a decrease in detrital grains and total organic carbon, and an increase in biogenic silica constituents, and were likely deposited at times of increased lake productivity during the dry season. We compare a floating varve chronology that spans ca. 2200 years with three radiocarbon-based age-depth models. Consistency between the varve chronology and one of the models partially supports the annual character of the laminated section in Lake Izabal. This laminated section, one of the first annually resolved sedimentological records from Central America, can help explore mid-Holocene hydroclimate variability and regional tectonic processes in this understudied region.

Keywords Elemental abundances · Varves · Lake Izabal · Lacustrine sediments · Guatemala · XRF-core scanner

Supplementary Information The online version contains supplementary material available at https://doi.org/10.1007/s10933-023-00292-x.

E. Duarte (✉) · J. Obrist-Farner
Geosciences and Geological and Petroleum Engineering Department, Missouri University of Science and Technology, Rolla, MO 65409, USA
e-mail: efdxkw@umsystem.edu

E. Duarte
EDYTEM, CNRS, Université Savoie Mont Blanc, Bâtiment Pôle Montagne, 73376 Le Bourget du Lac, France

S. R. H. Zimmerman
Center for Accelerator Mass Spectrometry, Lawrence Livermore National Laboratory, Livermore, CA 94550, USA

E. T. Brown · R. Brown
Large Lakes Observatory and Department of Earth and Environmental Sciences, University of Minnesota Duluth, Duluth, MN 55812, USA

Published online: 27 June 2023

Introduction

Paleolimnological investigations in Central America have highlighted the sensitivity of lake systems to past environmental, tectonic, and climatic changes (Leyden et al. 1994; Hodell et al. 1995, 2001; Curtis et al. 1996, 1998; Hillesheim et al. 2005; Mueller et al. 2009; Brocard et al. 2014; Wahl et al. 2014; Stansell et al. 2020). For example, several hydroclimate records indicate that Central America experienced relatively wet conditions during the early and mid-Holocene, followed by gradual drying during the late Holocene (Leyden et al. 1994; Hodell et al. 1995; Mueller et al. 2009; Wahl et al. 2014). This pattern of hydroclimate variability was interpreted as a response to a gradual shift in the mean position of the Intertropical Convergence Zone (ITCZ; Haug et al. 2001). Recent studies from the Guatemalan highlands, however, suggest that oceanic and atmospheric processes acting on much shorter time scales also significantly influenced Holocene hydroclimate in the region (Stansell et al. 2020; Winter et al. 2020). Additional highly resolved proxy records could provide key information to constrain sub-decadal and multi-decadal oceanic and atmospheric processes influencing precipitation in the region (Steinman et al. 2022; Obrist-Farner et al. 2023), such as the El Niño-Southern Oscillation (ENSO) and the North Atlantic Oscillation (NAO).

Laminated sediments are commonly preserved under meromictic lake conditions with strong seasonal contrasts and in absence of bioturbation, post-depositional erosion, re-suspension, and re-deposition (Ojala et al. 2012; Zolitschka et al. 2015). Although annually resolved (varved) laminated records can be found worldwide (Ojala et al. 2012; Ramisch et al. 2020), only a few varved records have been reported in Central America and the Caribbean region (Hughen et al. 1996; Brocard et al. 2014). Here we report on the sedimentology of a record from Lake Izabal, located in the eastern lowlands of Guatemala (Fig. 1), which was potentially deposited seasonally (i.e., varved). If the laminations are indeed varves, Lake Izabal will be a valuable location for high-resolution quantitative paleoclimatic and tectonic reconstructions in Central America and the Caribbean during that period.

Although Lake Izabal is currently shallow and well-mixed, a marine transgression during the early Holocene established a chemocline that turned Lake Izabal into a meromictic lake, with persistent bottom-water anoxia that lasted approximately 3500 years, from ca. 8370 to ca. 4800 cal year BP (Obrist-Farner et al. 2022). Anoxia decreased bioturbation in the deeper parts of the basin, facilitating preservation of a sequence of thinly laminated sediments (Duarte et al. 2021). Despite preliminary research results suggesting that the laminated sediment interval could be varved (Buckley and Obrist-Farner 2019), limited chronological constraints and difficulties in establishing correlations between overlapping cores have hampered a robust examination of the laminated section and the processes that led to their formation.

This study integrates sedimentological, radiocarbon age-depth modeling, smear-slide analysis, laminae counting, μX-ray fluorescence (μXRF) scanning, loss on ignition, and multivariate statistical analysis from a 400-cm-thick thinly laminated silty clay section collected from two sediment cores retrieved from the deepest part of Lake Izabal (Fig. 1). We use these analyses to demonstrate the annual character of the laminations and provide an improved chronology for the laminated interval. Laminations are sedimentologically and geochemically distinct, with differences in color, thickness, grain size, composition, and biogenic and organic matter content.

Geological background

Lake Izabal, located in the eastern lowlands of Guatemala, is a shallow lake with a surface area of 672 km^2 (Fig. 1). It occupies the eastern side of the Lake Izabal Basin, a pull-apart basin that developed ~ 12 Myr ago along the North American-Caribbean plate boundary (Bartole et al. 2019; Obrist-Farner et al. 2020). The lake has a catchment area of ~ 8740 km^2 and it is bounded by the Santa Cruz Mountain Range to the north, the Minas Mountain Range to the south, and the Mico Mountains to the east (Fig. 1). The watershed contains a variety of rocks and units, with the northern part composed of early Cretaceous ophiolitic units, partially serpentinized and heavily weathered, with sporadic carbonate sections (Mota-Vidaure 1989; Rosenfeld 1993). The southern part is mostly composed of Paleozoic metamorphic rocks, Cretaceous ophiolitic units, Cretaceous carbonate rocks, and Permian limestone. The eastern part is

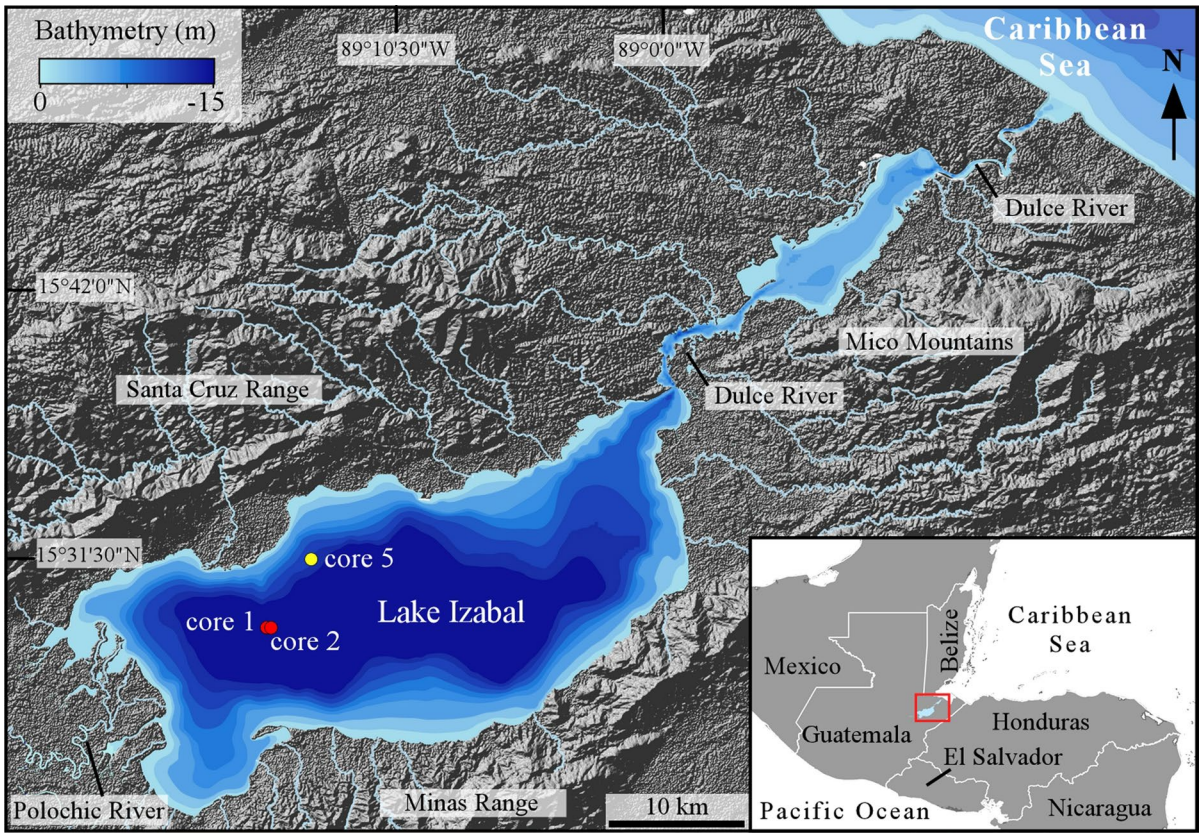

Fig. 1 Location of Lake Izabal showing the bathymetry of the lake and the main topographic features. Red dots show the locations of the two sediment cores (cores 1 and 2) used in this study. Yellow dot shows the location of sediment core 5 mentioned in the text. The bathymetric contour lines represent 2 m intervals. Inset map shows the location of the study area (red square) in the eastern lowlands of Guatemala

relatively rich in Carboniferous clastic rocks, Permian limestone, Cretaceous carbonate rocks, and Neogene strata exposing the initial infill of the basin (Mota-Vidaure 1989; Obrist-Farner et al. 2020).

Climate and hydrology

Lake Izabal is a polymictic and hydrologically open lake with a maximum water depth of 15 m (Fig. 1). The main tributary is the Polochic River, contributing ~ 70% of the water input to the lake (Brinson and Nordlie 1975; Obrist-Farner et al. 2019). The water-residence time in the lake is ~ 6 months, and the lake drains into the Caribbean Sea via the Dulce River (Brinson and Nordlie 1975; Fig. 1). Precipitation in Lake Izabal is seasonal, with a May to December rainy season, and a January to April dry season leading to an annual mean precipitation of ~ 3300 mm (Duarte et al. 2021). Modern limnological observations indicate that the lake is highly sensitive to precipitation seasonality (Brinson 1973; Brinson and Nordlie 1975). For example, during the wet season, lake level increases (maximum of 1.5 m; Medina et al. 2009) and increased runoff delivers abundant terrigenous sediment and allochthonous organic detritus to the lake (Brinson 1973). In contrast, during the dry season, decreased river input results in lower lake levels, lower terrigenous sediment input, and phytoplankton blooms (Brinson 1973; Brinson and Nordlie 1975; Medina et al. 2009). Paleolimnological studies have also illustrated that this system responds to long-term changes in nutrient input, erosion, precipitation, and sea-level changes (Obrist-Farner et al. 2019, 2022, 2023; Duarte et al. 2021; Mongol et al. 2023). In summary, seasonal climate variability, driven

mainly by the seasonal migration of the ITCZ, has significant effects on lake-level variations, lake productivity, and sediment and organic matter input into the lake.

Materials and methods

Two parallel and overlapping sediment cores (cores 1 and 2), ~ 6 m apart, were retrieved in 2018 from the deepest area of Lake Izabal using a modified Livingstone corer (Deevey 1965). Because of rough weather conditions, the uppermost unconsolidated mud-water interface sediments were not collected. Consolidated sediment sections (individual drives of 1 m) were collected at 185 cm below the lake-sediment surface for core 1 (15° 28′ 47.95" N, 89° 15′ 34.26" W) and 225 cm below the lake-sediment surface for core 2 (15° 28′ 48.08" N, 89° 15′ 34.10" W). The sediment cores (555 cm for core 1 and 470 cm for core 2) were kept in their polycarbonate-core tubes, sealed, and shipped to the University of Florida.

Magnetic susceptibility (MS) was measured at 0.5 cm resolution using a loop sensor in an automated core logger (Geotek MSCL-S). Then, sediment cores were split lengthwise, and cleaned core surfaces were scanned at 20 pixels mm^{-1} to acquire line-scan images using a Geotek Geoscan at the University of Florida. The working halves of the split cores were shipped to Missouri S&T for initial core description, while the other split halves were stored at the Land Use and Environmental Change Institute (LUECI) at the University of Florida. The initial core description was carried out by visual inspection of the cleaned core surfaces and the digital core-scan images following the protocol outlined by Schnurrenberger et al. (2003). We constructed a composite-sediment profile via cross-correlation of the line-scan images using Schlumberger's Techlog® 2017.2 software. The lithological description facilitated identification of three sedimentary zones and 38 stratigraphic laminae markers, which could be correlated between cores, to develop a spliced sequence that eliminated sediment intervals at the top of each core drive with evidence of disturbance caused while coring (Supplementary Figure [SF] 1; SF 2).

To characterize laminae composition and structure, we analyzed thin sections and smear slides, and measured grain size and carbon content. Thin sections were prepared from sediment slabs from core 1 at the Continental Scientific Drilling (CSD) Facility at the University of Minnesota Twin Cities using the freeze-drying technique of Normandeau et al. (2019). First, sediment slabs (7 × 2.5 cm) were submerged in liquid nitrogen dioxide (NO_2) and subsequently freeze-dried for four days. Slabs were then impregnated with Spurr resin and thin sections were prepared following standard techniques. Smear slides were prepared from untreated sediment and mounted into glass slides with Norland Optical Cement 61. Percent carbon (wt% C) was measured for 20 samples using a Carlo-Erba elemental analyzer at LUECI. Samples of dried bulk sediment (3 mg per sample) were analyzed from 623.8 to 625.7 cm of core 1. Grain-size distribution was determined for 10 samples in the laminated interval of core 1. To avoid contamination from nearby laminations, sampling was carried out in the central part of the laminae using a micro spatula and ~ 2 mg per sample was collected. Grain-size distribution was measured on a Microtrac S3500 laser diffraction particle analyzer at Missouri S&T with sonication to avoid particle flocculation. Two 30 s runs were carried out for each sample. Grain-size distributions are reported as mean grain size (M_z) with one standard deviation (Folk and Ward 1957).

Micro X-ray fluorescence (μXRF) core scanning was conducted on both cores at 0.5 mm steps. Because the laminations in the Izabal cores are, in some intervals, thinner than 0.5 mm, we scanned one impregnated thin section chip (from 520 to 517 cm) at 0.04 mm steps. The μXRF measurements were performed with an ITRAX™ core scanner at the Large Lakes Observatory at the University of Minnesota-Duluth, using a Cr X-ray source, operated at 30 kV and 55 mA and with a 15-s dwell time. The ITRAX™ core-scanner beam is 20 × 0.2 mm, with 0.2 mm in the sample-length direction; therefore, the 0.04 mm resolution scan has overlapping steps, with each step exposing 0.04 mm of new material (of the 0.20 mm sampling footprint). Measured elemental abundances are reported in total counts (tc), and elemental ratios are reported on a log scale to avoid ratio asymmetry (Weltje and Tjallingii 2008). Principal component analysis (PCA) was performed to summarize the relationship between elemental variables, where vector length indicates the amount of variance of each element and angles among vectors indicating their association (Jolliffe 1986). Elemental

counts were standardized (as z-scores) before PCA analysis to avoid confounding effects of dimensional heterogeneity.

Chronological control for both cores was established using accelerator mass spectrometry (AMS) radiocarbon (^{14}C) ages of five wood fragments. Samples were pretreated with standard acid–base-acid chemistry at the Center for Accelerator Mass Spectrometry (CAMS, Lawrence Livermore National Laboratory) and at Beta Analytic. Radiocarbon ages were combined into a composite-core chronology through the established stratigraphic correlation between the cores. Since the radiocarbon ages are not in stratigraphic order, we constructed three possible radiocarbon age-depth models using the Bacon package in R (Blaauw and Christen 2011) with the IntCal20 calibration curve (Reimer et al. 2020). Radiocarbon dates are in calibrated years before present (cal year BP) and are reported with the modeled 95% confidence range. The probability distribution of each calibrated age from the age-depth models was used with a Markov Chain Monte Carlo (MCMC) approach to produce a series of potential age models for the laminated section (Blaauw 2010). We extracted 1000 Monte-Carlo age-depth iterations for each of the three radiocarbon models using the Bacon package in R (Blaauw and Christen 2011) and plotted them using the MATLAB software.

The varve chronology for the composite core was established using a manual approach and a semi-automatic counting method. Manual counts were performed by one person using high-resolution line-scan images and measured in the software Techlog 2017.2. Manual counting uncertainty was established by replicating varve counts and thickness measurements along five different core segments (5 cm per segment) and providing five iterations for each segment. An estimate of counting error was calculated following Ji et al. (2021), by subtracting the maximum and the minimum number of counted varves and dividing the results by the average number of varves. Semi-automated varve counting was carried out using countMYvarves, a varve counting toolbox (Van Wyk de Vries et al. 2021). CountMYvarves uses sliding-window autocorrelation to count the number of repeated patterns in core-scan images and provides multiple independent counts (five iterations along each of 12 different transects) to evaluate counting uncertainty (Van Wyk de Vries et al. 2021). CountMYvarves uses as input parameters the resolution of the digital image (20 pixels mm^{-1}) and the estimated sedimentation rate (estimated to be 0.8 ± 0.02 mm year^{-1}; Obrist-Farner et al. 2022). Finally, a comparison of manual and semi-automatic varve-counting methods was undertaken. An estimated age at each point along the core depth for the thinly laminated zone was established based on the cumulative thickness of the manual laminae counts and the median of all the models performed by countMYvarves. Similarities between the varve chronology and the range of radiocarbon age-depth models generated with Bacon were used to assess the potential annual character of the laminated interval.

Results

Core sedimentology and geochemistry

The core contains three sedimentological zones: (1) homogeneous to bedded mud; (2) thinly bedded mud; and (3) thinly laminated mud. We focus here on the thinly laminated mud zone, which is 351 cm thick in core 1 and 325 cm thick in core 2 (Fig. 2). The thinly laminated mud zone is characterized by low MS (~5 SI) relative to overlying sediments (Fig. 2). This zone is also characterized by low and relatively constant Ti abundances while S abundances show the opposite pattern (Fig. 2; SF 3). Silica and Fe abundances have similar patterns, with highly variable abundances (SF 3). This variability is also observed in elemental ratios. For example, the log(S/Ti) ratio is characterized by high values, while the log(Si/Ti) ratio is characterized by a slightly upward increasing trend (Fig. 2). The most conspicuous feature of the thinly laminated mud zone is the consistent presence of dark and light laminae, which are very similar in thickness but differ in their color. For example, dark laminae are composed of dark grayish brown silty clay (10YR 4/2), while light laminae are composed of light brownish gray silty clay (10YR 6/2). Dark laminae have a mean thickness of 0.67 mm and a thickness range of 0.39–0.79 mm (Fig. 3), while light laminae have a mean thickness of 0.62 mm and a thickness range from 0.39 to 0.77 mm. Light and dark laminae couplets have a mean thickness of 1.28 mm and a thickness range of 0.85–1.55 mm (Fig. 3).

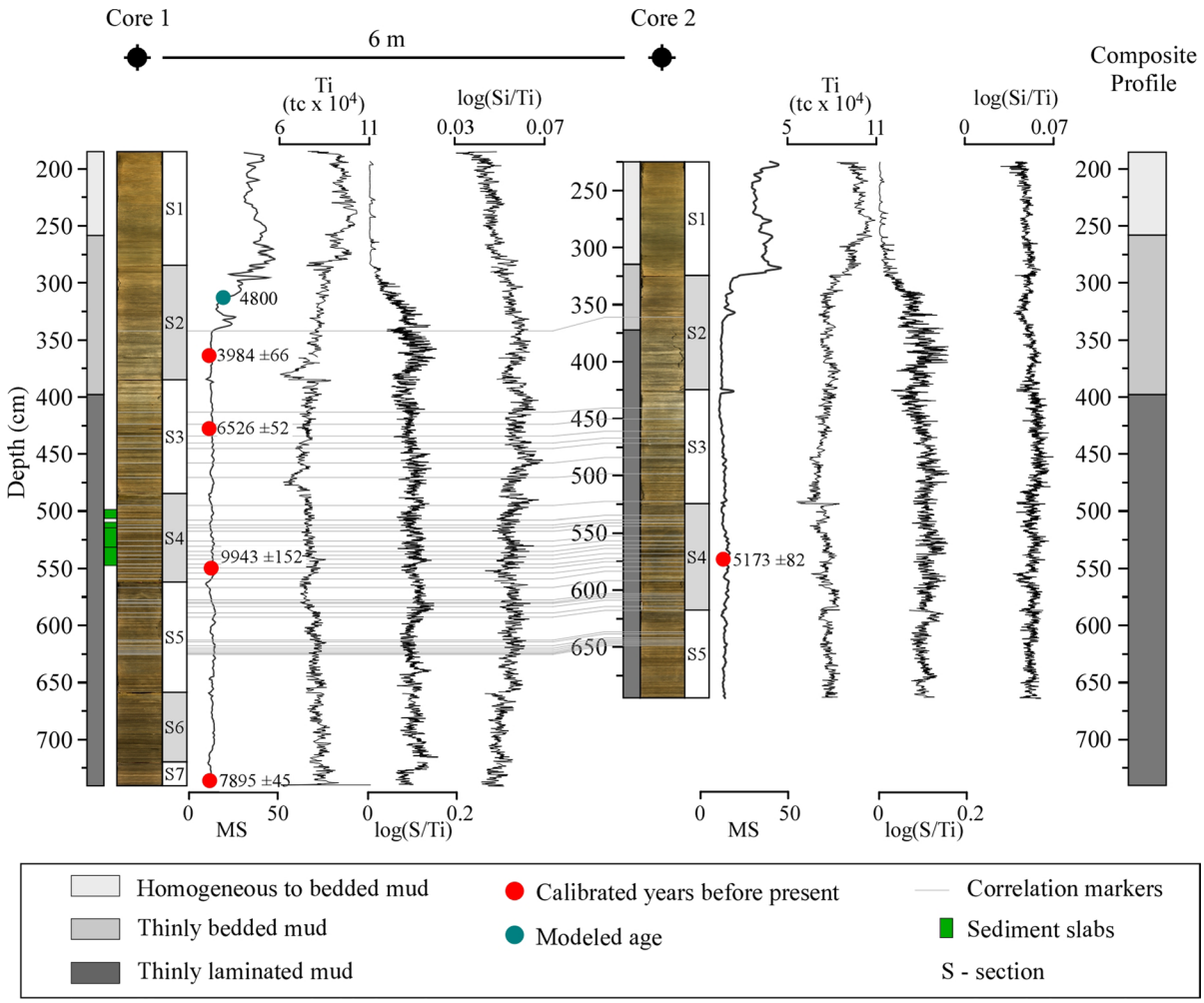

Fig. 2 Simplified lithological description, magnetic susceptibility (MS), titanium (Ti), and the log(S/Ti) and log(Si/Ti) ratios of the two sediment cores retrieved from Lake Izabal. Sediment cores were correlated using 38 laminae markers (gray lines). MS is expressed in international standard units (SI) and Ti is expressed in total counts (tc). Radiocarbon dates for cores 1 and 2 are in calibrated years before present (cal year BP). The sections (S) represent the individual sediment drives retrieved from Lake Izabal

Observations, including high-resolution line-scan images, microscopic analysis of smear slides, and grain-size measurements, indicate that the dark and light laminae are sedimentologically different. Dark laminae contain a larger proportion of detrital minerals (i.e., quartz, plagioclase) and terrestrial organic matter constituents, such as plant-cuticle fragments and amorphous organic matter (Fig. 4). Dark laminae also contain low abundances of lacustrine biogenic constituents, such as diatom fragments and sponge spicules, and contain a relatively high total carbon content (1.90–2.25 wt% C; Supplementary Table [ST] 1) and a high abundance of microscopic pyrite grains (Fig. 4). Dark laminae have a mean grain size of medium silt ($M_z = 0.026$ mm ± 0.008; $n = 5$) and are composed of $6.98 \pm 3.70\%$ clay, $78.41 \pm 5.92\%$ silt, and $15.21 \pm 7.72\%$ sand (SF 4). In contrast, light laminae are characterized by a lower abundance of detrital minerals and organic matter constituents, are enriched in biogenic constituents, and contain a relatively lower total carbon content (1.31–1.77 wt% C; ST 1) and moderate abundances of microscopic pyrite grains (Fig. 4). Light laminae have a mean grain size of fine silt ($M_z = 0.010$ mm ± 0.002; $n = 5$) and are

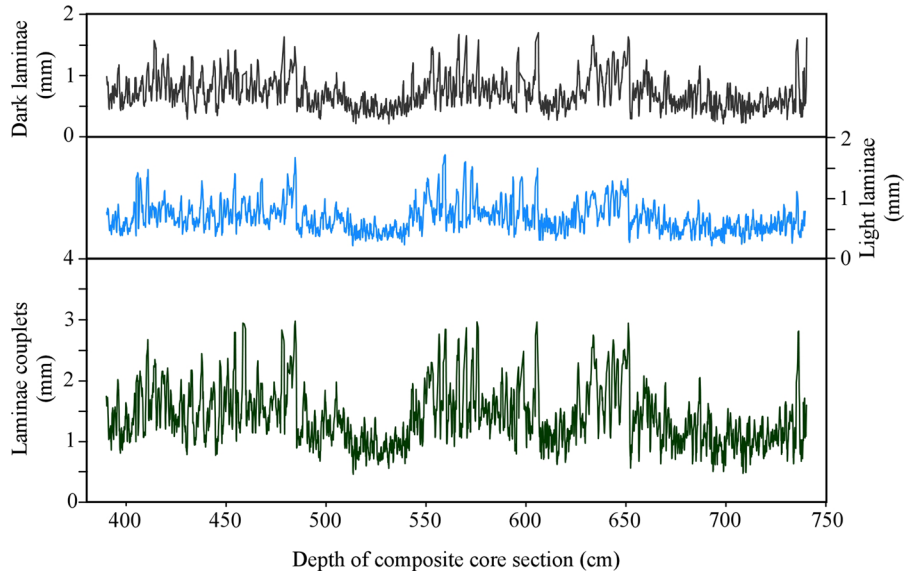

Fig. 3 Measured thickness for dark and light laminae and laminae couplets for the thinly laminated mud zone

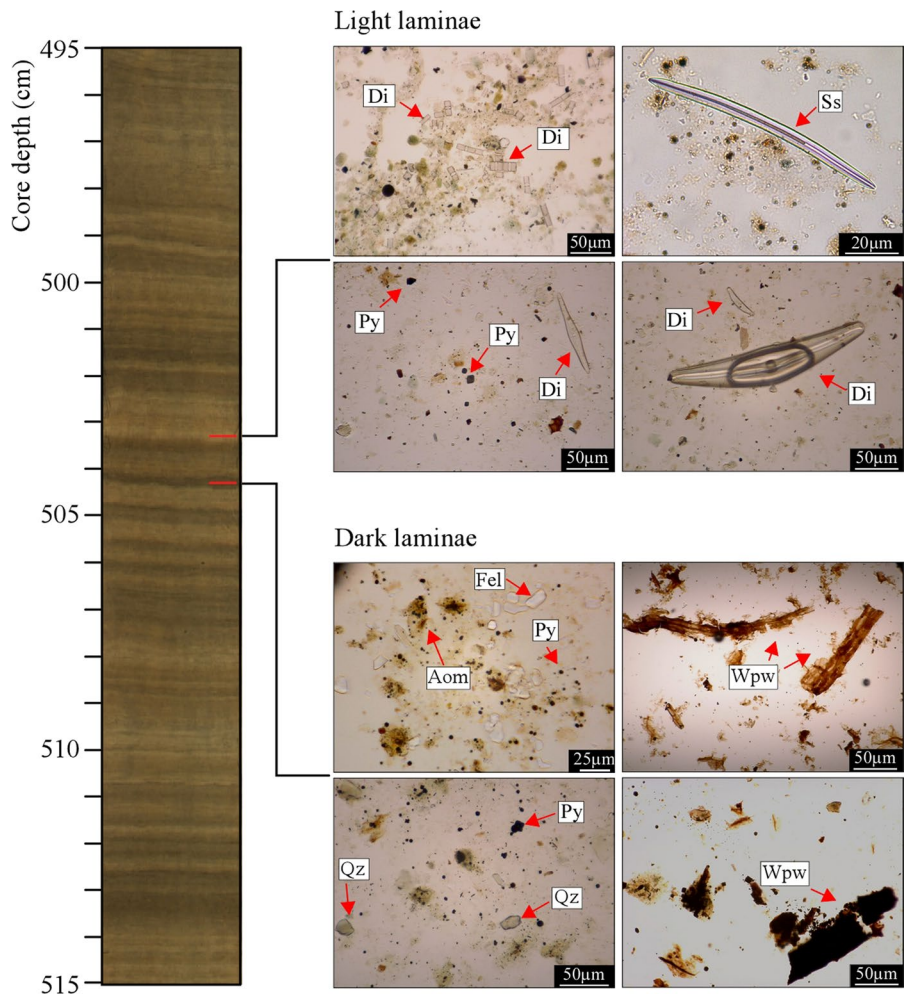

Fig. 4 High-resolution digital core-scan image showing a section of the thinly laminated mud zone in core 1. Photomicrographs showing an example of light and dark laminae highlighting the main components of the laminae. All images were taken under plane-polarized light. Qz—Quartz; Fel – Feldspar; Py—Pyrite; Ss—Sponge spicule; Di—Diatom; Aom—Amorphous organic matter; Wpw – Well-preserved wood fragment

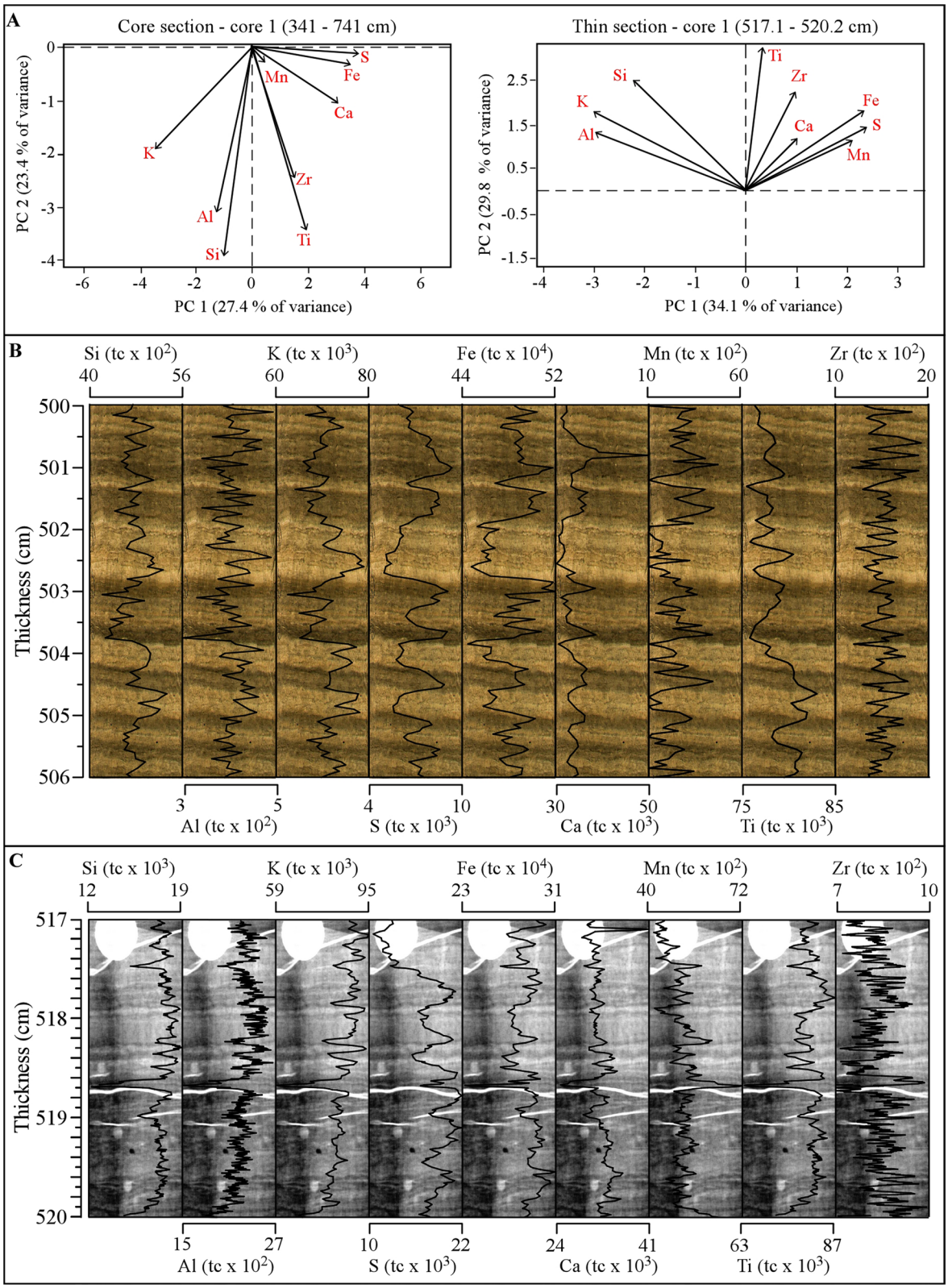
A
Core section - core 1 (341 - 741 cm)
PC 2 (23.4 % of variance)
PC 1 (27.4 % of variance)
S
Fe
Mn
Ca
K
Zr
Al
Si
Ti
Thin section - core 1 (517.1 - 520.2 cm)
PC 2 (29.8 % of variance)
PC 1 (34.1 % of variance)
Ti
Si
Zr
K
Fe
Ca
Al
S
Mn
B
Si (tc x 10²)
K (tc x 10³)
Fe (tc x 10⁴)
Mn (tc x 10²)
Zr (tc x 10²)
Thickness (cm)
Al (tc x 10²)
S (tc x 10³)
Ca (tc x 10³)
Ti (tc x 10³)
C
Si (tc x 10³)
K (tc x 10³)
Fe (tc x 10⁴)
Mn (tc x 10²)
Zr (tc x 10²)
Thickness (cm)
Al (tc x 10²)
S (tc x 10³)
Ca (tc x 10³)
Ti (tc x 10³)

◂**Fig. 5** **a** Principal component analyses (PCA) for element abundances in the thinly laminated mud zone for core 1 (left) and thin section chip (right). **b** Digital core-scan image with elemental abundances in total counts (tc) for a section of the thinly laminated mud zone in core 1. **c** Thin section radiographs (darker is higher density) showing elemental abundances in tc for the thin section chip from core 1

composed of 16.22 ± 4.75% clay, 76.38 ± 3.88% silt, and 7.40 ± 8.51% sand (SF 4).

X-ray fluorescence results from the cores and thin section chip, combined with PCA results, indicate that the dark laminae are characterized by a high abundance of Ti, Fe, S, Mn, Zr, and Ca. In contrast, light laminae contain higher abundances of Si, K, and Al (Fig. 5). PCA of the μXRF data shows three main modes of variability. The first mode of variability is a relationship between S, Fe, Mn, and Ca, which are associated along the positive side of the principal component 1 (PC1) in core 1 (27.4% of variance), along the positive side of PC2 in core 2 (27.6% of variance; SF 5), and along the positive side of PC 1 in the thin section (34.1% of variance; Fig. 5). The second mode of variability is the relationship between Si, K, and Al, which are associated along the negative side of PC2 in core 1 (23.4% of variance), along the negative side of PC1 in core 2 (33.9% of variance; SF 5), and along the negative side of PC1 in the thin section (34.1% of variance; Fig. 5). The third mode of variability is a relationship between Ti and Zr, which are between the two main modes of variability in both cores and thin sections (Fig. 5; SF 5).

Elemental ratios also show that the laminae are distinctly different. For example, dark laminae in the cores and thin section chip are characterized by high log(Fe/Ti), log(Mn/Ti), log(Zr/K), and log(S/Ti) ratios (Fig. 6). Light laminae, on the other hand, are characterized by high log(Si/Ti) and log(Al/Ti) ratios (Fig. 6). The PCA results on the ratios indicate a relationship between log(Fe/Ti), log(Mn/Ti), and log(S/Ti), which are associated along the positive axis of PC2 in the core section, explaining 26.3% of the variance (Fig. 6). In contrast, the log(Si/Ti), log(Al/Ti), and log(Zr/K) ratios are statistically different and are aligned to the PC1 axis, which explains 43.8% of the variance. The log(Si/Ti) and log(Al/Ti) ratios are aligned to the negative axis and the log(Zr/K) ratio is align to the positive axis of PC1. Similarly, XRF ratios on the thin section chip are characterized by a relationship between log(Mn/Ti), log(Fe/Ti), and log(S/Ti) ratios, which are associated with the positive axis of PC2 (28.1% of variance). In contrast, log(Si/Ti), log(Al/Ti), and log(Zr/K) ratios are associated with PC1 (44.9% of variance). The log(Si/Ti) and log(Al/Ti) ratios are aligned to the negative axis and the log(Zr/K) ratio is align to the positive axis of PC1 (Fig. 6).

Radiocarbon-based chronology

The radiocarbon ages obtained in cores 1 and 2 are not in stratigraphic order, so their interpretation is not straightforward (Table 1). To examine the possible range of ages for the composite core, we generated three radiocarbon-based age-depth models with differing assumptions (Fig. 7). In addition to the radiocarbon ages, the age of 4800 cal year BP (95% range = 4520–5105) was added at 312 cm depth in the composite profile. This age is derived from the age-depth model of Duarte et al. (2021) for core 5 (6 km away from core 1; Fig. 1) and marks the transition from brackish to freshwater conditions in Lake Izabal (Duarte et al. 2021; Obrist-Farner et al. 2022). The transition between oxic and anoxic conditions is marked by a rapid increase in MS and Ti, and a rapid decrease in S and in the log(S/Ti) ratio after 312 cm depth in core 1 and 325 cm depth in core 2 (Fig. 2; SF 3, SF 5). Based on the lithostratigraphic correlation between core 5 and cores 1 and 2 of Obrist-Farner et al. (2022), the date was placed at 312 cm depth in the composite profile.

Model 1 utilizes three radiocarbon dates and suggests that the laminated segment of the composite profile could span ~ 3727 years, from 7875 (95% range = 7717–7995) to 4148 (95% range = 3949–4351) cal year BP (Fig. 7). Median sedimentation rates range from 0.09 to 0.12 cm year^{-1} from 740 to 547 cm and then increase to 0.13–0.17 cm year^{-1} between 547 and 389 cm (Fig. 8). Model 2 is based on two radiocarbon dates and the age of 4800 cal year BP (95% range is 4520–5105). Results indicate that the laminated segment of the composite profile could span ~ 2500 years, from 8325 (95% range = 7893–9221) to 5822 (95% range = 5510–6116) cal year BP (Fig. 7). Median sedimentation rates range from 0.15 to 0.22 cm year^{-1} from 740 to 435 cm, followed by a sharp decrease, ranging from 0.15 to 0.22 cm year^{-1} from 435 to 389 cm (Fig. 8). Model 3 is based on two

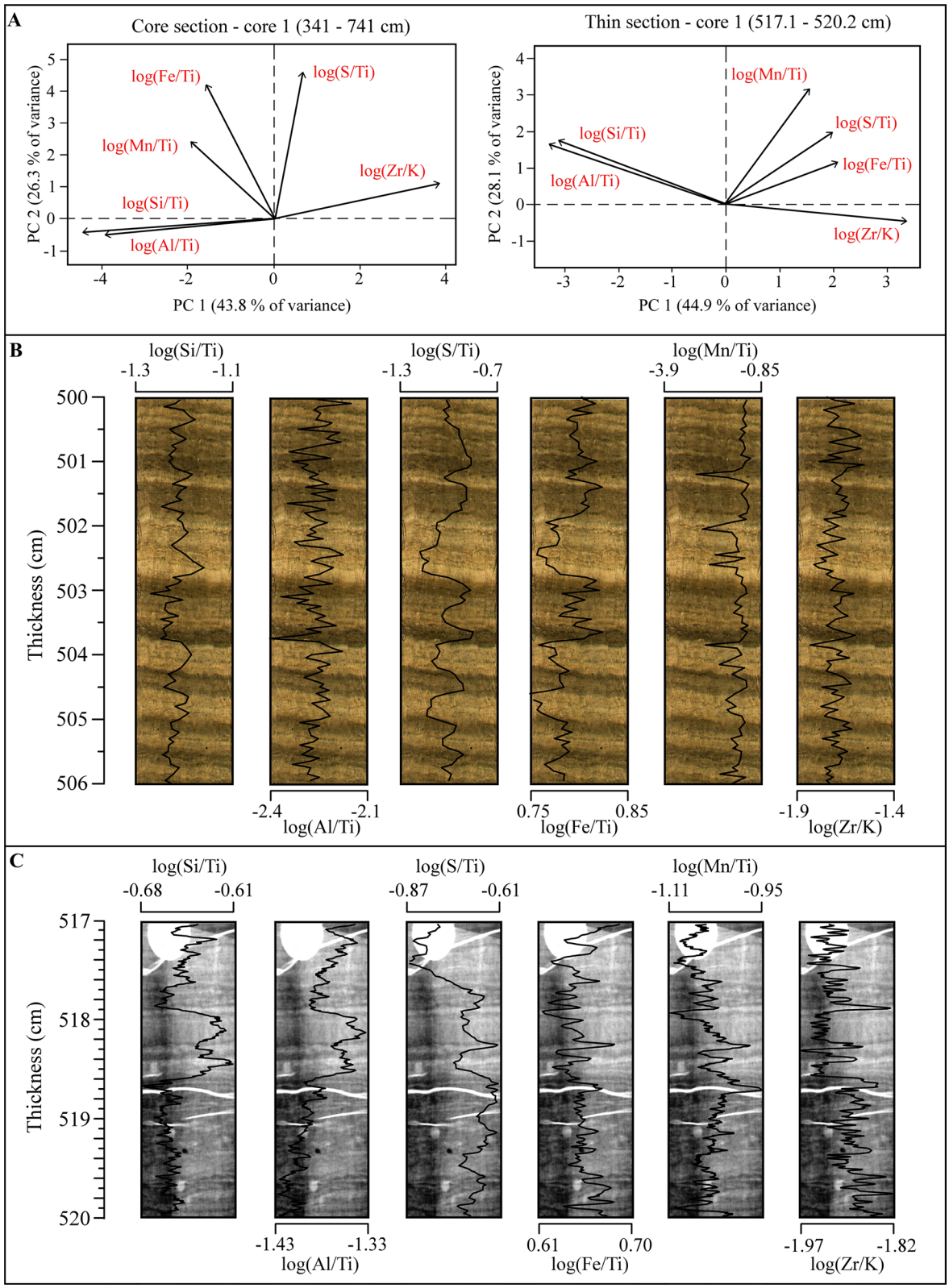
A
Core section - core 1 (341 - 741 cm)
log(Fe/Ti)
log(S/Ti)
log(Mn/Ti)
log(Zr/K)
log(Si/Ti)
log(Al/Ti)
PC 2 (26.3 % of variance)
PC 1 (43.8 % of variance)
Thin section - core 1 (517.1 - 520.2 cm)
log(Mn/Ti)
log(Si/Ti)
log(S/Ti)
log(Fe/Ti)
log(Al/Ti)
log(Zr/K)
PC 2 (28.1 % of variance)
PC 1 (44.9 % of variance)
B
log(Si/Ti)
-1.3
-1.1
log(S/Ti)
-1.3
-0.7
log(Mn/Ti)
-3.9
-0.85
Thickness (cm)
500
501
502
503
504
505
506
-2.4
-2.1
log(Al/Ti)
0.75
0.85
log(Fe/Ti)
-1.9
-1.4
log(Zr/K)
C
log(Si/Ti)
-0.68
-0.61
log(S/Ti)
-0.87
-0.61
log(Mn/Ti)
-1.11
-0.95
Thickness (cm)
517
518
519
520
-1.43
-1.33
log(Al/Ti)
0.61
0.70
log(Fe/Ti)
-1.97
-1.82
log(Zr/K)

◂**Fig. 6** **a** Principal component analyses for XRF ratios from the thinly laminated mud zone for core 1 (top) and thin section chip (bottom). **b** Digital core-scan image showing elemental ratios for a section of the thinly laminated mud zone in core 1. **c** Thin section radiograph (darker is higher density) showing elemental ratios for the thin section chip from core 1

calibrated radiocarbon dates. Results indicate that the laminated segment of the composite profile could span ~ 2422 years, from 6518 (6147–6926) to 4096 (3890 – 4288) cal year BP (Fig. 7). Median sedimentation rates remain constant throughout the laminated interval, ranging from 0.16 to 0.21 cm year^{-1} (Fig. 8).

Lamina counting and varved age-depth models

To evaluate the manual laminae counts, we compared the counts against the minimum, the maximum, and the median of all the models performed by countMYvarves (Fig. 9). Varve chronology, based on manual counts covers 2186 ± 114 years (Fig. 9). On the other hand, the varve chronology derived from countMYvarves covers 2102 years, with a maximum of 2187 years and a minimum of 2000 years (Fig. 9). We also compared the manual and semi-automated laminae-count models with 1000 MCMC age-depth models obtained from the three radiocarbon-based age-depth models (Fig. 10). The results for model 1 indicate that the sedimentation rate derived from the varve model is similar to the radiocarbon-based age-depth models until ~ 590 cm. However, this similarity breaks down in the lower 156 cm, with the varve model predicting a higher sedimentation rate (0.18 cm year^{-1}) than the radiocarbon-based age-depth model (0.09 cm year^{-1}). Models 2 and 3 have sedimentation rates (0.19 and 0.18 cm year^{-1}, respectively) comparable to that of the varve model (0.18 cm year^{-1}), with the varve-model ages coinciding with the lower age ranges of the MCMC results for both models 2 and 3 (Fig. 10).

Discussion

Laminae analysis

Our sedimentological observations reveal a detailed and well-preserved laminated core section in Lake Izabal (Fig. 9), covering a large part of the mid-Holocene. Our analyses indicate that the dark and light laminae are distinct, with differences in color, composition, texture, and organic constituents. The larger grain size and abundance of detrital grains and allochthonous woody organic fragments suggest that dark laminae formed during times of greater terrestrial sediment input into Lake Izabal. This inference is supported by a greater abundance of elements associated with increased runoff, such as Ti, Zr, and Fe (Davies et al. 2015; Fig. 5), as well as by a higher concentration of total organic carbon (ST 1) and higher log(S/Ti) ratio, a proxy for organic matter content (Moreno et al. 2007). The larger grain size is supported by higher abundance of Zr, which is typically higher in coarse silt and very fine sand that contain heavy minerals (Cuven et al. 2010). Our data suggest that the dark laminae were deposited during times of increased river runoff, most likely during the rainy season, consistent with modern observations that the hydrological regime exerts a significant control on organic matter and sediment flow into Lake Izabal, and that turbidity increases during the wet season with input of detritus-laden waters (Brinson 1973).

Light laminae, on the other hand, have smaller grain size, fewer detrital grains and lower organic

Table 1 Radiocarbon dates on samples from cores 1 and 2 in Lake Izabal, Guatemala

Sample type	Accession number	Core name	MCD (cm)	^{14}C age (year BP)	± 1σ	Mean age (cal year BP)[a]	Error (1σ)
Wood fragment	CAMS-185397	1	364	3645	40	3984	66
Wood fragment	Beta-504957	1	428	5730	30	6526	52
Wood fragment	Beta-516048	2	542	4530	30	5173	82
Wood fragment	CAMS-185398	1	552	8860	80	9943	152
Wood fragment	Beta-503614	1	739	7070	40	7895	45

[a]Radiocarbon ages at depth in the core were converted into calendar ages (cal year BP) using Oxcal 4.4 (Bronk Ramsey 2009) with the calibration curve IntCal20 (Reimer et al. 2020). MCD denotes master-composite depth

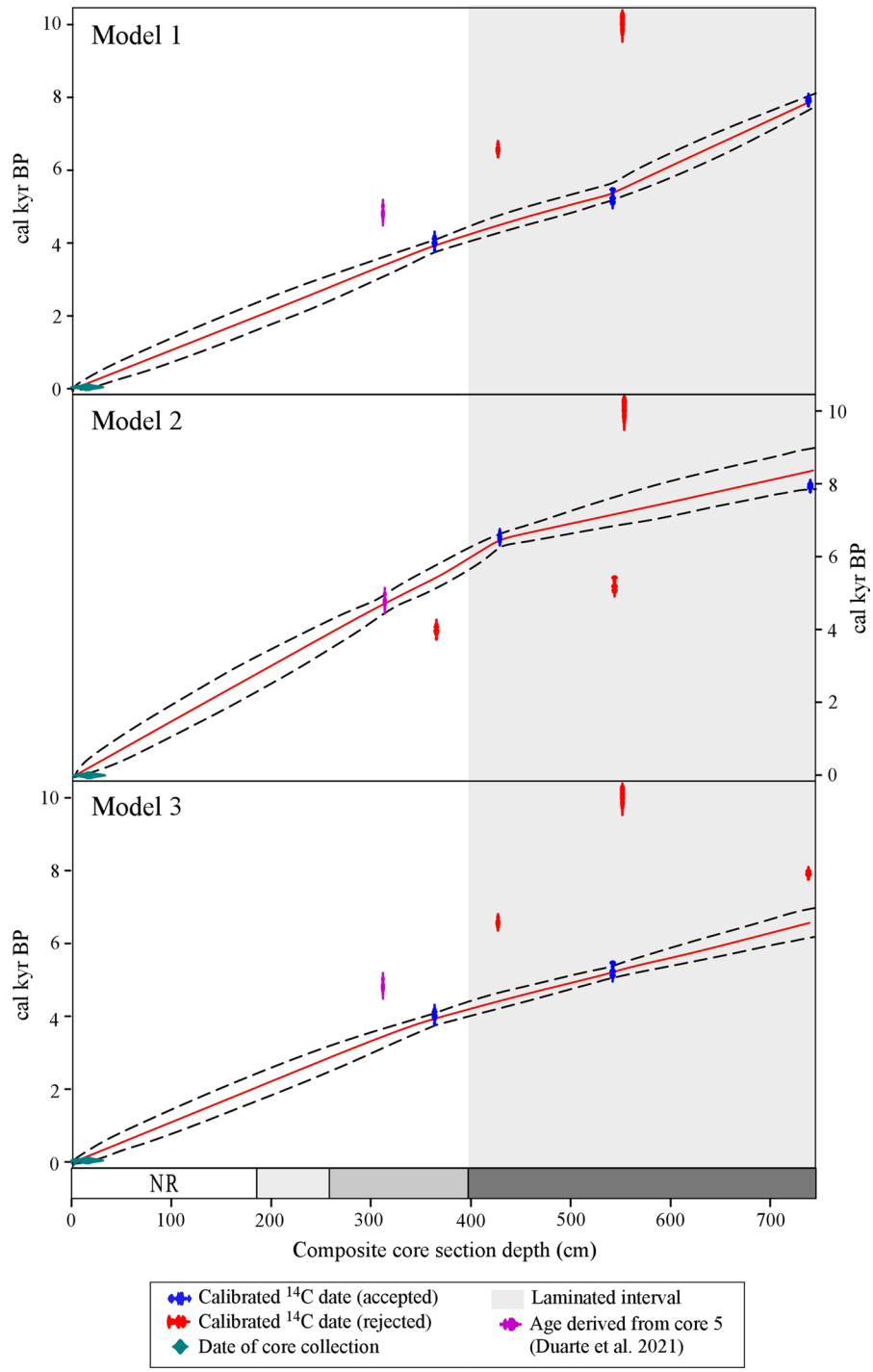

Fig. 7 Proposed age-depth models for the composite-core profile. Age-depth models were constructed using the Bayesian software Bacon (Blaauw and Christen 2011). Envelopes between black dashed lines show the 95% confidence intervals. Red curves show the single best model based on the mean age for each depth. See Fig. 2 for the simplified lithological legend. NR = core segment not recovered

content (ST 1), and a higher abundance of diatoms and sponge spicules (Fig. 4). These data suggest a reduction in detrital input to the lake associated with an increase in lake productivity. This is supported by an overall increase in Si and the log(Si/Ti) ratio (Fig. 6), indicating increased production and deposition of lacustrine biogenic silica (Brown et al. 2007; Brown 2011, 2015). The decrease in grain size is

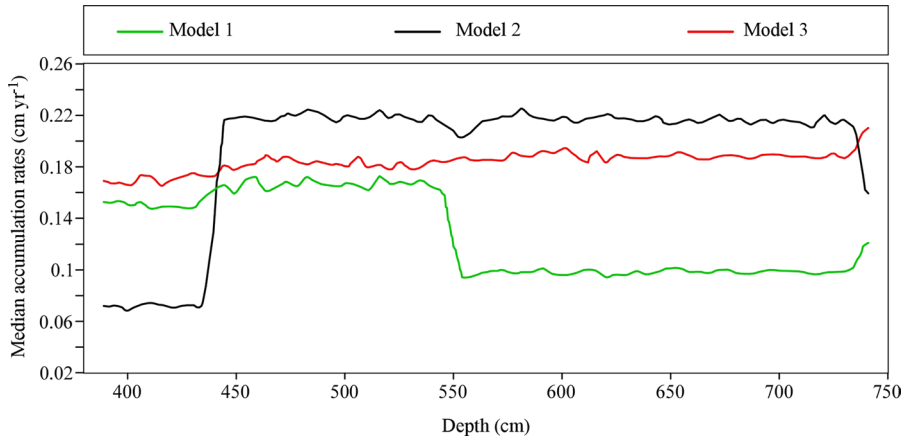

Fig. 8 Estimated median accumulation rates (cm year^{-1}) for the three proposed age-depth models. Accumulation rates were computed using the Bacon package in R (Blaauw and Christen 2011)

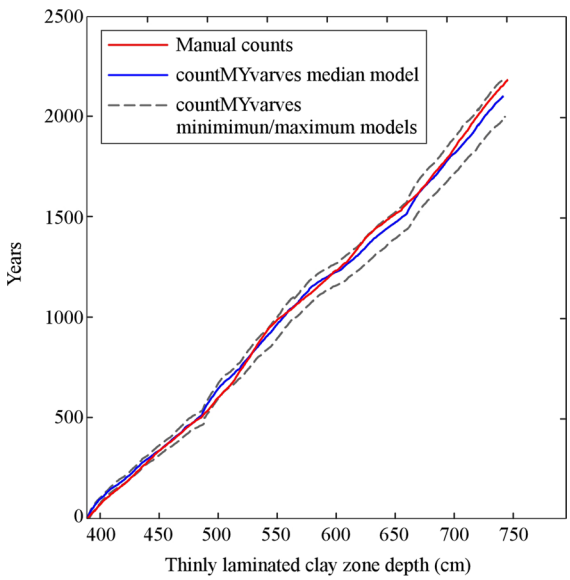

Fig. 9 Results of the manual laminae counts and the semi-automated models for the entire thinly laminated mud zone (lowermost 351 cm of the composite profile). The semi-automated models were generated using countMYvarves (Van Wyk de Vries et al. 2021)

supported by higher abundances of K and Al as these elements are associated with fine silt and clay layers (Cuven et al. 2010; Clift et al. 2014). Our inference is also supported by modern limnological observations in Lake Izabal that indicate increased primary productivity during the dry season (Brinson and Nordlie 1975), most likely as a result of greater light penetration in the water column due to decreased turbidity. In summary, our sedimentological observations most likely indicate that dark and light laminae formed in response to the seasonality in precipitation and were preserved during a time when Lake Izabal's bottom water was anoxic (Fig. 11).

Changes in the elemental composition of the laminae reveal additional biogeochemical processes that occurred during the mid-Holocene. For example, S and Fe covary, especially in the dark laminae, evidenced by their association in the PCA results (Fig. 5). In anoxic marine sediments, pyrite (FeS) formation is aided by the presence of sulfate-reducing bacteria and organic matter, which is necessary for sulfate reduction (Raiswell and Berner 1985). The higher concentration of organic carbon and woody debris, combined with bottom-water anoxia in Izabal, likely facilitated and enhanced pyrite formation within the dark laminae.

Throughout the thinly laminated mud zone, the observed changes in XRF elemental abundances do not systematically correlate with the observed changes in the core photographs. There are two potential reasons for this discrepancy. First, the µXRF core scans were carried out at 0.5 mm steps, while laminations in Lake Izabal are, on average, 0.64 mm thick but range between 0.39 and 0.78 mm. The variability in laminae thickness and constant 0.5 mm steps by the core scanner would have resulted in variable levels of aliasing. Second, the laminations in Lake Izabal are not always parallel to each other and are not always perpendicular to the core tube. The ITRAX has an 8-mm wide analytical footprint, so measurements from fine non-horizontal laminae could represent combined results from two or more laminae. The thin-section chip was analyzed at a much finer resolution (0.04 mm) to characterize the laminae at greater

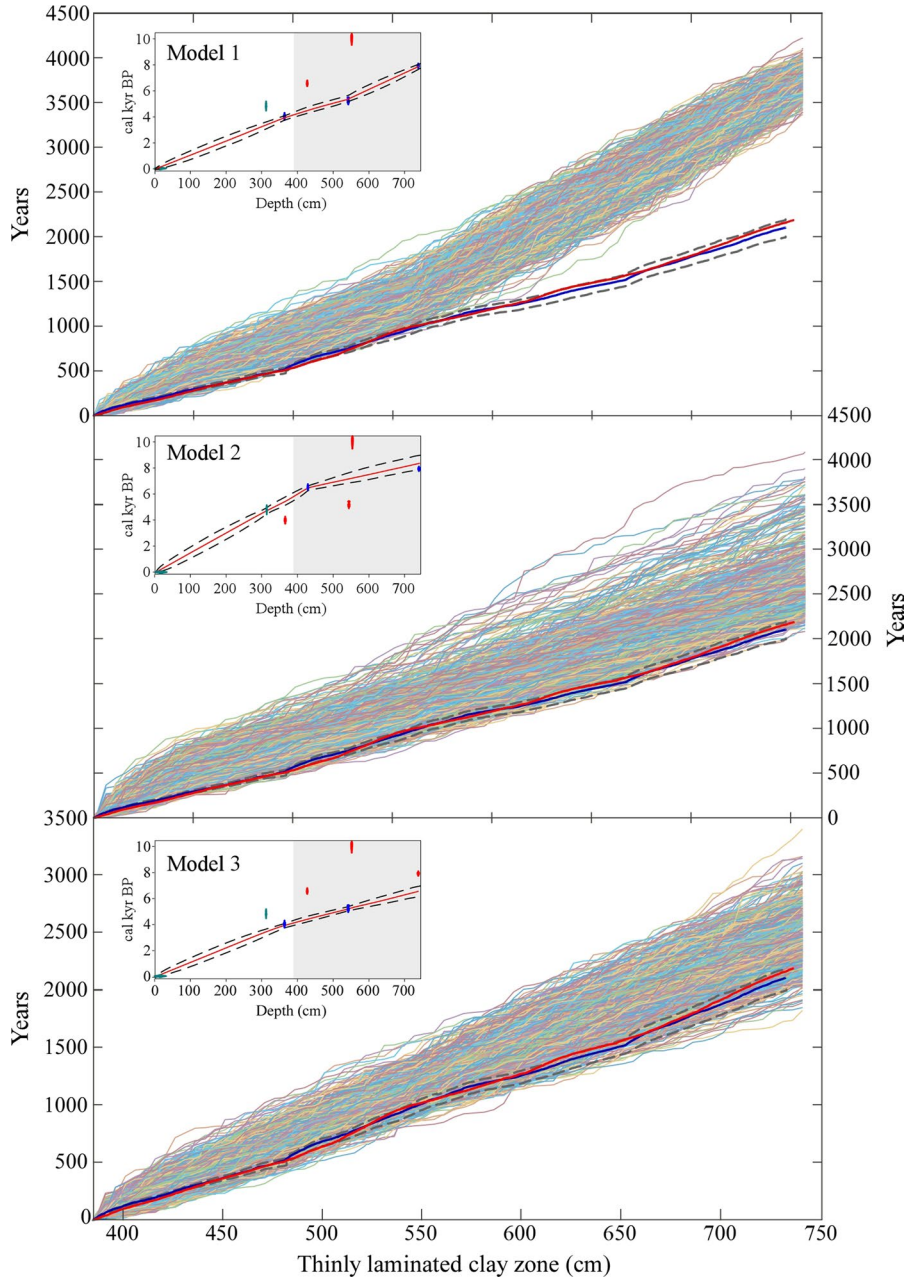

Fig. 10 1000 Markov Chain Monte Carlo (MCMC) age-depth iterations for the laminated section of the composite profile plotted with the varve chronology. The Monte Carlo iterations were extracted from the radiocarbon-based age-depth models calculated using the Bacon package in R (Blaauw and Christen 2011)

detail (Marshall et al. 2012), providing a better representation of the elemental variability of the laminae present in the sediment cores.

Age models: laminations as varves

Difficulties in obtaining radiocarbon ages throughout the core make it challenging to prove that the laminae couplets are annually deposited. However, the combination of previous knowledge of basin-wide geochemical changes (Obrist-Farner et al. 2022), three radiocarbon age-depth models, manual laminae counting, and the semi-automated varve-counting method allowed us to infer the annual character of the laminations. Similarities between the age-depth relationships established by our manual counts, the countMYvarves software, and radiocarbon age-depth models 2 and 3 provide evidence to support

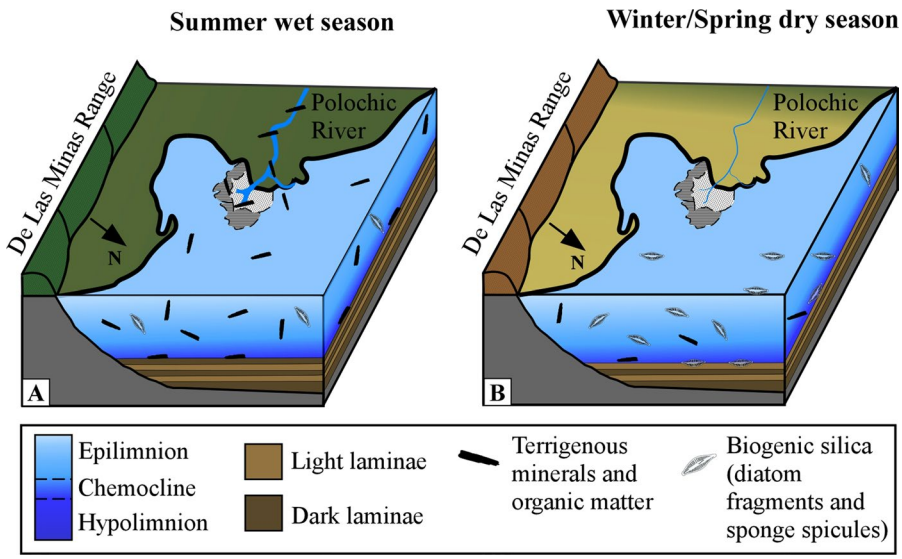

Fig. 11 Depositional model of the thinly laminated mud zone in Lake Izabal. **a** Deposition of dark laminae during the summer wet season, characterized by a high abundance of organic matter and detritus. **b** Deposition of light laminae during the winter and spring dry season, characterized by a high abundance of biogenic silica and reduced detritus

our interpretation of the laminae as varves. Further, our methodology helps reduce the time necessary to provide uncertainty estimations in manual laminae counts (Zolitschka et al. 2015; Żarczyński et al. 2018). For example, countMYvarves provides multiple simultaneous counts (i.e., five iterations along 12 different transects), which speeds up the counting process and improves the transparency and reproducibility of the results (Van Wyk de Vries et al. 2021). In our study, the manual counts are consistent with the semi-automated counting approach and are within the uncertainty calculated by the semi-automated model (Fig. 9). We show that by combining manual counts with the semi-automatic counting models from countMYvarves, laminae counting can be improved and corroborated, providing objective results that are less time-consuming.

The scarcity of macroscopic organic fragments and lack of stratigraphic order in our radiocarbon results led to substantial uncertainty in our age-depth models. Several processes could have resulted in the anomalous radiocarbon dates obtained from the two cores. Material that is older or younger than the surrounding sediment can be the result of sampling too close to the outside edge of the core; however, all of the dated wood fragments were obtained from the middle of the core where the laminations were intact. The penetration of roots from emergent or terrestrial vegetation down into the cored sediments can result in ages that are too young, but this is highly unlikely as the cores were collected in deep water and there is no evidence of root structures in the sediment. On the other hand, the anomalously old radiocarbon ages (e.g., 552 cm) in the three radiocarbon models (Fig. 7) could be attributed to the input of reworked old carbon material into the lake sediments. The introduction of old carbon material into younger sediment is a common feature in Lake Izabal (Obrist-Farner et al. 2019), especially in cores taken near the large wetland and river delta located in the western side of the lake (Fig. 1).

Despite the difficulties in establishing chronological constraints in cores 1 and 2, additional supporting information helped us discriminate between the possible chronologies for the laminated section. First, the presence of laminae in both cores and their thickness trends is inconsistent with abrupt changes in sedimentation rates within the laminated sections, required by both radiocarbon-based models 1 and 2. Deposition of laminae with similar thickness indicates that sedimentation rate was relatively constant during the mid-Holocene. A constant sedimentation rate for the laminated sediment section is also supported by the age-depth model and sedimentation rate from core 5 (Fig. 1; Duarte et al. 2021). Second, Duarte et al. (2021) reported a linear sedimentation rate of ~ 0.08 cm year^{-1} for the laminated segment of core 5 based on an age-depth model with 11 radiocarbon dates. This sedimentation rate is half of the one reconstructed based on radiocarbon age-depth models

2 and 3 and based on the varve-age-depth model. However, the laminated segment of cores 1 (351 cm) and 2 (325 cm) differ in thickness from the laminated segment of core 5 (210 cm), suggesting that the sediment rate in the deeper, more central part of Lake Izabal was at least twice as high as in the core 5 location. Changes in sedimentation rates and net accumulation for the deeper part of the basin can be related to sediment-focusing processes (Davis and Ford 1982) and to the proximity of cores 1 and 2 to the large delta of the Polochic River (Fig. 1). Finally, model 2 includes a date of 4800 cal year BP assigned to the transition from persistent bottom-water anoxia to oxic bottom waters at the shallower core 5 site (Duarte et al. 2021; Obrist-Farner et al. 2022). Interestingly, exclusion of the 4800 cal year BP date from model 3 increases the similarity between the radiocarbon age-depth model and the varve model (Fig. 10). This suggests that the change from brackish to freshwater might not have occurred at the same time in the deeper parts of the basin. Instead, our results suggest that the change may have been gradual, with the brackish to freshwater transition occurring ~ 730 years later in the deeper part of Lake Izabal. One plausible explanation for the gradual change from brackish to freshwater conditions is the differences in water depth between coring sites. Gradual erosion of the chemocline by the constant input of freshwater into Lake Izabal would have resulted in time-transgressive changes from anoxic to oxic waters, with shallower coring sites (i.e., core 5 location) gradually changing to freshwater conditions earlier than those in the deeper part of the basin (cores 1 and 2).

In conclusion, our results support our inference that the laminated intervals of cores 1 and 2 are varves and that radiocarbon model 3 is the most plausible, based on the dates in hand. The implied changes in sedimentation rates in both radiocarbon-based models 1 and 2 are not supported by our sedimentological observations. Additionally, the likelihood of the introduction of young carbon is low in the laminated segment of the Izabal cores. It is likely, however, that older carbon-bearing materials from the Polochic wetland were introduced into the system and transported to the deeper parts of Lake Izabal. If these inferences are correct, the laminated segment of Izabal cores 1 and 2 spans around ca. 2200 years based on our floating varve chronology, spanning from ~ 6300 to ~ 4100 cal year BP, thus providing the first mid-Holocene annually laminated sedimentological record from the northern Neotropics.

Conclusions

Sedimentological and geochemical analyses of thinly laminated intervals in sediment cores from Lake Izabal provide new insights into the nature and chronology of the laminations and the processes that led to their formation. The laminated section consists of alternating clastic (dark) and biogenic (light) laminae couplets that are distinctly different in their color, texture, and composition. These couplets most likely formed by the characteristic seasonality in precipitation observed in western Central America and were preserved during a time when Lake Izabal's bottom water was anoxic. Despite uncertainty in our radiocarbon age-depth models, multiple lines of evidence presented here suggest that the laminae couplets are varves. Additional cores and radiocarbon dates would help to further refine and constrain the chronology of the laminae. Nonetheless, this work provides a detailed view of the sedimentary, geochemical, and biological processes that led to the formation of the laminae in Izabal, documenting one of the first annually resolved sedimentological records from the region spanning the mid-Holocene.

Acknowledgements The authors thank Steffen Mischke and two anonymous reviewers for their constructive reviews that significantly improved the quality of this manuscript. We thank Defensores de la Naturaleza Foundation (Guatemala) and the Continental Scientific Drilling (CSD) Facility at the University of Minnesota Twin Cities for help with core collection and analyses, respectively. This is contribution # 15 of the Missouri S&T MCTF research group, and LLNL-JRNL-805149.

Author contribution ED, and JOF contributed to data collection, sedimentological analysis, results interpretation, and manuscript preparation. SZ contributed to geochronological analysis. EB, and RB contributed to geochemical analysis. All authors contributed to results interpretation and editing of the manuscript.

Funding This study was partially supported by the Geological Society of America (GSA) Graduate Student Research Grant to ED, funded by the National Science Foundation (NSF) Award No. 1712071. This research was also partially supported by the Visiting Graduate Student Program from the Continental Scientific Drilling (CSD) Facility (Minnesota) to ED and by NSF Award no. 2029102 to JOF.

Declarations

Conflict of interest The authors declare that they have no known competing financial interests or personal relationships that could have appeared to influence the work reported in this paper.

References

Bartole R, Lodolo E, Obrist-Farner J, Morelli D (2019) Sedimentary architecture, structural setting, and Late Cenozoic depocentre migration of an asymmetric transtensional basin: Lake Izabal, eastern Guatemala. Tectonophysics 750:419–433. https://doi.org/10.1016/j.tecto.2018.12.004

Blaauw M (2010) Methods and code for 'classical' age-modelling of radiocarbon sequences. Quat Geochronol 5:512–518. https://doi.org/10.1016/j.quageo.2010.01.002

Blaauw M, Christen JA (2011) Flexible paleoclimate age-depth models using an autoregressive gamma process. Bayesian Anal 6:457–474. https://doi.org/10.1214/11-BA618

Brinson MM (1973) The organic matter budget and energy flow of a tropical lowland aquatic ecosystem. University of Florida, New York

Brinson MM, Nordlie FG (1975) II. Lakes. 8. Central and South America: Lake Izabal, Guatemala. SIL Proceedings, 1922–2010 Internationale Vereinigung für Theoretische und Angewandte Limnologie. Verhandlungen 19:1468–1479. https://doi.org/10.1080/03680770.1974.11896206

Brocard G, Adatte T, Magand O, Pfeifer HR, Bettini A, Arnaud F, Anselmetti FS, Moran-Ical S (2014) The recording of floods and earthquakes in Lake Chichój, Guatemala during the twentieth century. J Paleolimnol 52:155–169. https://doi.org/10.1023/10.1007/s10933-014-9784-4

Bronk Ramsey CB (2009) Bayesian analysis of radiocarbon dates. Radiocarbon 51:337–360. https://doi.org/10.1017/S0033822200033865

Brown E (2011) Lake Malawi's response to "megadrought" terminations: Sedimentary records of flooding, weathering and erosion. Palaeogeogr Palaeoclimatol Palaeoecol 303:120–125. https://doi.org/10.1016/j.palaeo.2010.01.038

Brown E (2015) Estimation of biogenic silica concentrations using scanning XRF: insights from studies of Lake Malawi sediments. In: Smol JP (ed) Micro-XRF studies of sediment cores applications of a non-destructive tool for the environmental sciences. Springer, Ontario, pp 267–277. https://doi.org/10.1007/978-94-017-9849-5_9

Brown E, Johnson TC, Scholz C, Cohen A, King J (2007) Abrupt change in tropical African climate linked to the bipolar seesaw over the past 55,000 years. Geophys Res Lett 34:L20702. https://doi.org/10.1029/2007GL031240

Buckley KL, Obrist-Farner J (2019) Sedimentological characteristics of a laminated core from Lake Izabal, eastern Guatemala. Geological Society of America Annual Meeting, Phoenix, Arizona, USA, vol 51, No 5, Paper 193-10. https://doi.org/10.1130/abs/2019AM-336341

Clift PD, Wan S, Blusztajn J (2014) Reconstructing chemical weathering, physical erosion and monsoon intensity since 25Ma in the northern South China Sea: a review of competing proxies. Earth Sci Rev 130:86–102. https://doi.org/10.1016/j.earscirev.2014.01.002

Curtis JH, Hodell DA, Brenner M (1996) Climate variability on the Yucatan Peninsula (Mexico) during the past 3500 years, and implications for Maya cultural evolution. Quat Res 46:37–47. https://doi.org/10.1006/qres.1996.0042

Curtis JH, Brenner M, Hodell DA, Balser RA, Islebe GA, Hooghiemstra H (1998) A multi-proxy study of Holocene environmental change in the Maya Lowlands of Peten, Guatemala. J Paleolimnol 19:139–159. https://doi.org/10.1023/A:1007968508262

Cuven S, Francus P, Lamoureux SF (2010) Estimation of grain size variability with micro X-ray fluorescence in laminated lacustrine sediments, Cape Bounty, Canadian High Arctic. J Paleolimnol 44:803–817. https://doi.org/10.1007/s10933-010-9453-1

Davies SJ, Lamb H, Roberts S (2015) Micro-XRF core scanning in palaeolimnology: Recent developments. In: Croudace I, Rothwell R (eds) Micro-XRF studies of sediment cores. Developments in paleoenvironmental research, vol 17. Springer, Dordrecht, pp 189–226. https://doi.org/10.1007/978-94-017-9849-5_7

Davis MB, Ford MS (1982) Sediment focusing in Mirror Lake, New Hampshire. Limnol Oceanogr 27:137–150. https://doi.org/10.4319/lo.1982.27.1.0137

Deevey ES (1965) Sampling lake sediments by use of the Livingstone sampler. In: Kummel B, Raup D (eds) Handbook of paleontological techniques. Freeman, New York, pp 521–529. https://doi.org/10.1002/gj.3350050122

Duarte E, Obrist-Farner J, Correa-Metrio A, Steinman BA (2021) A progressively wetter early through middle Holocene climate in the eastern lowlands of Guatemala. Earth Planet Sci Lett 561:116807. https://doi.org/10.1016/j.epsl.2021.116807

Folk RL, Ward WC (1957) Brazos River bar [Texas] a study in the significance of grain size parameters. J Sediment Res 27:3–26. https://doi.org/10.1306/74D70646-2B21-11D7-8648000102C1865D

Haug GH, Hughen KA, Sigman DM, Peterson LC, Röhl U (2001) Southward migration of the Intertropical Convergence Zone through the Holocene. Science 293:1304–1308. https://doi.org/10.1126/science.1059725

Hillesheim MB, Hodell DA, Leyden BW, Brenner M, Curtis JH, Anselmetti FS, Ariztegui D, Buck DG, Guilderson TP, Rosenmeier MF (2005) Climate change in lowland Central America during the late deglacial and early Holocene. J Quat Sci 20:363–376. https://doi.org/10.1002/jqs.924

Hodell DA, Curtis JH, Brenner M (1995) Possible role of climate in the collapse of Classic Maya civilization. Nature 375:391–394. https://doi.org/10.1038/375391a0

Hodell DA, Brenner M, Curtis JH, Guilderson T (2001) Solar forcing of drought frequency in the Maya lowlands. Science 292:1367–1370. https://doi.org/10.1126/science.1057759

Hughen KA, Overpeck JT, Peterson LC, Anderson RF (1996) The nature of varved sedimentation in the Cariaco Basin, Venezuela and its palaeoclimatic significance. In: Kemp AES (ed) Palaeoclimatology and palaeoceanography from

laminated sediments, vol 16. Geological Society Special Publicatin, London, pp 171–183. https://doi.org/10.1144/GSL.SP.1996.116.01.15

Ji K, Zhu E, Chu G, Aquino-López MA, Hou J (2021) A record of late Holocene precipitation on the Central Tibetan Plateau inferred from varved lake sediments. J Paleolimnol 66:439–452. https://doi.org/10.1007/s10933-021-00215-8

Jolliffe I (1986) Principal component analysis. Springer, Berlin. https://doi.org/10.1007/b98835

Leyden BW, Brenner M, Hodell DA, Curtis JH (1994) Orbital and internal forcing of climate on the Yucatan Peninsula for the past ca. 36 ka. Palaeogeogr Palaeoclimatol Palaeoecol 109:193–210. https://doi.org/10.1016/0031-0182(94)90176-7

Marshall M, Schlolaut G, Nakagawa T, Lamb H, Brauer A, Staff R, Ramsey CB, Tarasov P, Gotanda K, Haraguchi T, Yokoyama Y (2012) A novel approach to varve counting using μXRF and X-radiography in combination with thin-section microscopy, applied to the Late Glacial chronology from Lake Suigetsu, Japan. Quat Geochronol 13:70–80. https://doi.org/10.1016/j.quageo.2012.06.002

Medina C, Gomez-Enri J, Villares P, Alonso J (2009) An Integrated methodology for the environmental assessment and management of Lake Izabal (Guatemala). In: Proceedings of the 3rd WSEAS International Conference on Energy Planning, Energy Saving, Environmental Education, pp 150–157

Mongol E, Oboh-Ikuenobe F, Obrist-Farner J, Moreno JE, Correa-Metrio A (2023) A millennium of anthropic and climate dynamics in the Lake Izabal Basin, eastern lowland Guatemala. Rev Palaeobot Palynol 312:104872. https://doi.org/10.1016/j.revpalbo.2023.104872

Moreno A, Giralt S, Valero-Garcés B, Sáez A, Bao R, Prego R, Pueyo JJ, González-Sampériz P, Taberner C (2007) A 14kyr record of the tropical Andes: the Lago Chungará sequence (18°S, northern Chilean Altiplano). Quat Int 161:4–21. https://doi.org/10.1016/j.quaint.2006.10.020

Mota-Vidaure ABY (1989) Stratigraphy of the coal-bearing strata (Miocene) in the Carboneras region, Izabal, Guatemala. Colorado School of Mines, New York

Mueller AD, Islebe GA, Hillesheim MB, Grzesik DA, Anselmetti FS, Ariztegui D, Brenner M, Curtis JH, Hodell DA, Venz KA (2009) Climate drying and associated forest decline in the lowlands of northern Guatemala during the late Holocene. Quat Res 71:133–141. https://doi.org/10.1016/j.yqres.2008.10.002

Normandeau A, Brown O, Jarrett K, Francus P, De Coninck A (2019) Epoxy impregnation of unconsolidated marine sediment core subsamples for the preparation of thin sections at the Geological Survey of Canada (Atlantic). Geolog Surv Can Tech Note 10:10. https://doi.org/10.4095/313055

Obrist-Farner J, Brenner M, Curtis JH, Kenney W, Salvinelli C (2019) Recent onset of eutrophication in Lake Izabal, the largest water body in Guatemala. J Paleolimnol 62:359–372. https://doi.org/10.1007/s10933-019-00091-3

Obrist-Farner J, Eckert A, Locmelis M, Crowley JL, Mota-Vidaure B, Lodolo E, Rosenfeld J, Duarte E (2020) The role of the Polochic Fault as part of the North American and Caribbean Plate boundary. Insights from the infill of the Lake Izabal Basin. Basin Res 32:1347–1364. https://doi.org/10.1111/bre.12431

Obrist-Farner J, Brenner M, Stone JR, Wojewódka-Przybył M, Bauersachs T, Eckert A, Locmelis M, Curtis JH, Zimmerman SRH, Correa-Metrio A, Schwark L, Duarte E, Schwalb A, Niewerth E, Echeverría-Galindo PG, Pérez L (2022) New estimates of the magnitude of the sea-level jump during the 8.2 ka event. Geology 50:86–90. https://doi.org/10.1007/10.1130/g49296.1

Obrist-Farner J, Steinman BA, Stansell ND, Maurer J (2023) Incoherency in Central American hydroclimate proxy records spanning the last millennium. Paleoceanogr Paleoclimatol 38:e2022PA004445. https://doi.org/10.1029/2022PA004445

Ojala AEK, Francus P, Zolitschka B, Besonen M, Lamoureux SF (2012) Characteristics of sedimentary varve chronologies—a review. Quat Sci Rev 43:45–60. https://doi.org/10.1016/j.quascirev.2012.04.006

Raiswell R, Berner RA (1985) Pyrite formation in euxinic and semi-euxinic sediments. Am J Sci 285:710–724. https://doi.org/10.2475/ajs.285.8.710

Ramisch A, Brauser A, Dorn M, Blanchet C, Brademann B, Köppl M, Mingram J, Neugebauer I, Nowaczyk N, Ott F (2020) VARDA (VARved sediments DAtabase)–providing and connecting proxy data from annually laminated lake sediments. Earth Syst Sci Data 12:2311–2332. https://doi.org/10.5194/essd-12-2311-2020

Reimer PJ, Austin WEN, Bard E, Bayliss A, Blackwell PG, Bronk Ramsey C, Butzin M, Cheng H, Edwards RL, Friedrich M, Grootes PM, Guilderson TP, Hajdas I, Heaton TJ, Hogg AG, Hughen KA, Kromer B, Manning SW, Muscheler R, Palmer JG, Pearson C, van der Plicht J, Reimer RW, Richards DA, Scott EM, Southon JR, Turney CSM, Wacker L, Adolphi F, Büntgen U, Capano M, Fahrni SM, Fogtmann-Schulz A, Friedrich R, Köhler P, Kudsk S, Miyake F, Olsen J, Reinig F, Sakamoto M, Sookdeo A, Talamo S (2020) The IntCal20 northern hemisphere radiocarbon age calibration curve (0–55 cal kBP). Radiocarbon 62:725–757. https://doi.org/10.1017/RDC.2020.41

Rosenfeld JH (1993) Sedimentary Rocks of the Santa Cruz ophiolite, Guatemala–a proto-Caribbean history. In: Pindell JL, Perkins BF (eds) Mesozoic and Early Cenozoic development of the Gulf of Mexico and Caribbean region—a context for hydrocarbon exploration. SEPM Society for Sedimentary Geology. https://doi.org/10.5724/gcs.92.13

Schnurrenberger D, Russell J, Kelts K (2003) Classification of lacustrine sediments based on sedimentary components. J Paleolimnol 29:141–154. https://doi.org/10.1023/A:1023270324800

Stansell ND, Steinman BA, Lachniet MS, Feller J, Harvey W, Fernandez A, Shea CJ, Price B, Coenen J, Boes M, Perdziola S (2020) A lake sediment stable isotope record of late-middle to late Holocene hydroclimate variability in the western Guatemala highlands. Earth Planet Sci Lett 542:116327. https://doi.org/10.1016/j.epsl.2020.116327

Steinman BA, Stansell ND, Mann ME, Cooke CA, Abbott MB, Vuille M, Bird BW, Lachniet MS, Fernandez A (2022) Interhemispheric antiphasing of neotropical

precipitation during the past millennium. Proc Natl Acad Sci 119:e2120015119. https://doi.org/10.1073/pnas.2120015119

Wahl D, Byrne R, Anderson L (2014) An 8700 year paleoclimate reconstruction from the southern Maya lowlands. Quat Sci Rev 103:19–25. https://doi.org/10.1016/j.quascirev.2014.08.004

Weltje GJ, Tjallingii R (2008) Calibration of XRF core scanners for quantitative geochemical logging of sediment cores: theory and application. Earth Planet Sci Lett 274:423–438. https://doi.org/10.1016/j.epsl.2008.07.054

Winter A, Zanchettin D, Lachniet M, Vieten R, Pausata FSR, Ljungqvist FC, Cheng H, Edwards RL, Miller T, Rubinetti S, Rubino A, Taricco C (2020) Initiation of a stable convective hydroclimatic regime in Central America circa 9000 years BP. Nat Commun 11:716–732. https://doi.org/10.1038/s41467-020-14490-y

Wyk V, de Vries M, Ito E, Shapley M, Brignone G (2021) Semi-automated counting of complex varves through image autocorrelation. Quat Res 104:89–100. https://doi.org/10.1017/qua.2021.10

Żarczyński M, Tylmann W, Goslar T (2018) Multiple varve chronologies for the last 2000 years from the sediments of Lake Żabińskie (northeastern Poland)–comparison of strategies for varve counting and uncertainty estimations. Quat Geochronol 47:107–119. https://doi.org/10.1016/j.quageo.2018.06.001

Zolitschka B, Francus P, Ojala AEK, Schimmelmann A (2015) Varves in lake sediments—a review. Quat Sci Rev 117:1–41. https://doi.org/10.1038/s41467-020-14490-y

Publisher's Note Springer Nature remains neutral with regard to jurisdictional claims in published maps and institutional affiliations.

Springer Nature or its licensor (e.g. a society or other partner) holds exclusive rights to this article under a publishing agreement with the author(s) or other rightsholder(s); author self-archiving of the accepted manuscript version of this article is solely governed by the terms of such publishing agreement and applicable law.